

Catalysis Science & Technology

Accepted Manuscript



This is an *Accepted Manuscript*, which has been through the Royal Society of Chemistry peer review process and has been accepted for publication.

Accepted Manuscripts are published online shortly after acceptance, before technical editing, formatting and proof reading. Using this free service, authors can make their results available to the community, in citable form, before we publish the edited article. We will replace this *Accepted Manuscript* with the edited and formatted *Advance Article* as soon as it is available.

You can find more information about *Accepted Manuscripts* in the [Information for Authors](#).

Please note that technical editing may introduce minor changes to the text and/or graphics, which may alter content. The journal's standard [Terms & Conditions](#) and the [Ethical guidelines](#) still apply. In no event shall the Royal Society of Chemistry be held responsible for any errors or omissions in this *Accepted Manuscript* or any consequences arising from the use of any information it contains.



Study on the origin of the active sites of HDN catalysts using alumina-supported MoS₃ nanoparticles as a precursor

Wei Han*, Hong Nie, Xiangyun Long, Mingfeng Li, Qinghe Yang, Dadong Li

Received 00th January 20xx,
Accepted 00th January 20xx

DOI: 10.1039/x0xx00000x

www.rsc.org/

This article proposes alumina-supported MoS₃ nanoparticles (NPs) as a precursor of model catalysts to study catalytic mechanisms of hydrodenitrogenation (HDN). The NPs were first loaded into γ -Al₂O₃ by a simple chemical deposition method and then thermally treated under atmosphere H₂, N₂ and H₂S, respectively, to obtain three MoS₂/Al₂O₃ catalysts. XPS, N₂ adsorption-desorption and HRTEM characterization results show, using MoS₃ NPs instead of conventional MoO_x NPs as the precursor can effectively tune the edge composition of the MoS₂ phase while controlling its micromorphology and avoiding the strong interference to it from the alumina support, thus laying the foundation of accurately understanding the origin of the active sites for HDN reactions. Then the catalytic activity of the series MoS₃-derived catalysts were thoroughly studied and comprehensive results are obtained after rationally deducing the “structure-function” relations: (i) two type active sites exist in the HDN catalysts, one for hydrogenation reaction which is related with both sulfur vacancies and brim sites and another for C-N hydrogenolysis reaction which is connected with the -SH/S²⁻ groups on the edge of the active phase; (ii) the edge composition directly influences the Ni-promoting effect and the “sulfur-deficient” edge structure is more beneficial for Ni promoter role. Due to the actual catalyst model first used, the resulting viewpoints exhibit valuable guiding significance for high-efficient HDN catalyst development.

Keywords: MoS₃ nanoparticles, MoS₂, hydrodenitrogenation catalyst, edge composition, active site, hydrogenation, hydrogenolysis

Introduction

In recent years, hydrodenitrogenation (HDN) has been gaining more importance due to the continuously growing environmental concerns and increasing needs for processing heavy oils and low-quality feeds which contain larger quantities of nitrogen compounds than the traditional petroleum oils.^{1, 2} During hydroprocessing, HDN occurs simultaneously with hydrodesulfurization (HDS), hydrodeoxygenation (HDO), hydrodearomatization (HDA) and hydrodemetallization (HDM), however, unfortunately, due to the nitrogen-compounds' generally preferential adsorption on the potential catalytic sites, HDN often strongly inhibits the other reactions and thereby results in the undesirable process efficiency, such as a difficulty to attain the ultra-low level of sulfur required by fuel specifications.³⁻⁶ In various HDN processes, the catalysts play a pivotal role in determining process efficiency and the development of more active HDN catalysts has become the most cost-effective approach.^{7, 8} A better understanding the “structure-function” relation and the

origin of the active sites of the catalysts can apparently accelerate the development process.

As the most important type of hydrotreating catalysts, alumina-supported molybdenum disulfide (MoS₂) nanocrystallines or nanoparticles (NPs) usually promoted by Co or Ni atoms have been used in the refining industry for more than half a century.⁹⁻¹¹ Extensive studies generally agreed that,^{4, 12-14} only the edge sites (generally divided into Mo-edge and S-edge) of MoS₂ NPs exhibit catalytic activity and the basal plane is inactive. Furthermore, by virtue of scanning tunneling microscopy (STM) analysis, Topsøe and his co-workers recently successfully obtained insight into the detailed atomic structure of the edges and pointed that,^{15, 16} except for the extensively acceptable sulfur vacancies which contribute to the catalytic activity (coordinatively unsaturated sites, CUS, likely located at the S-edge), there exists a special metallic brim site along the Mo-edge with a coordinatively saturated state but exhibiting potential catalytic activity, as proved by the later studies.^{17, 18} Therefore, the potential catalytic active sites are nothing but related to CUS sites, -SH/S²⁻ groups and brim-Mo sites on or near the edges of the MoS₂ active phase. However, how the three type potential active sites contribute to various hydroprocessing reactions, especially the usual most complicated HDN, is still undergoing widespread controversy.

It is well accepted that, due to the more difficult for C=N bond breaking than C-N bond, HDN reactions first have to

Research Institute of Petroleum Processing, SINOPEC, 18 Xue Yuan Road, 100083 Beijing, PR China. E-mail: hanwei.ripp@sinopec.com

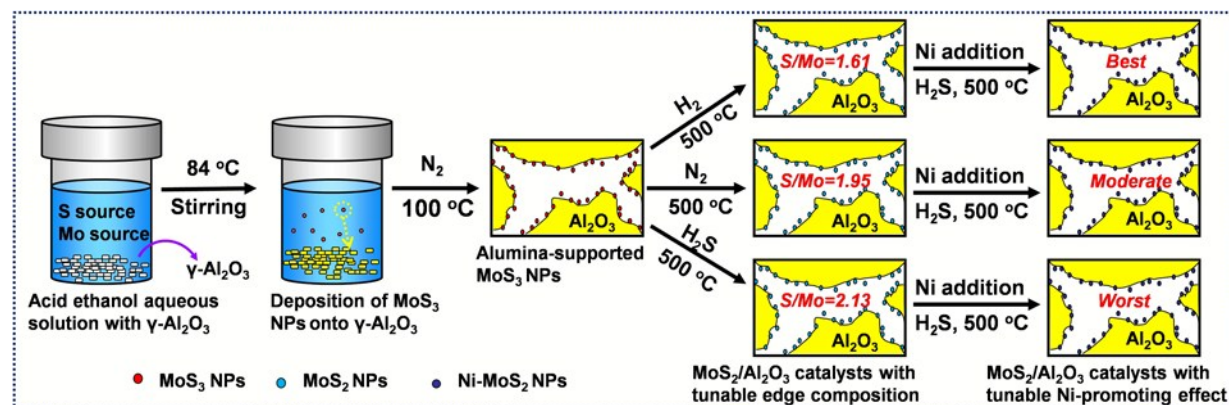
† Electronic Supplementary Information (ESI) available: HDS and HDN activity of the conventional catalyst IM-CAT and the three MoS₃-derived monometallic catalysts, and Q conversion and product selectivity over the three MoS₃-derived catalysts as a function of the reaction temperature. See DOI: 10.1039/x0xx00000x

proceed heterocyclic ring hydrogenation and then the C-N bond cleavage can take place.^{1, 3} Hence, balanced dual functional active sites on a HDN catalyst are essential: one for hydrogenation pathway, noted as HYD, another for C-N hydrogenolysis pathway, noted as DN.^{4, 19} Generally, most of the researchers pointed out there exist two type of active sites:^{3, 4, 20, 21} CUS and proton acid center (H^+) or $-SH$ species, the former was considered as the HYD active site; whereas the latter which is ascribed to B acid site was taken for the DN or isomerization center, and these two sites can transform from each other in the presence of both H_2 and H_2S .^{4, 22} Except for the CUS site accounting for HYD reactions, until recently, the far-reaching results obtained by Topsøe's team showed that the brim sites together with their neighboring acidic protons interact strongly with N-containing molecules and the HYD reactions could also take place in the brim sites, which now has been often used to rationally explain the strong inhibition effect of the N-containing molecules on the HDS reactions.¹⁸ For DN reactions, so far, Hofmann elimination and nucleophilic substitution are still the most two extensively accepted reaction mechanisms of C-N bond breaking, but both consider the B acid sites ($-SH$ species) as the active sites.^{3, 4, 23} Most recently, Gutiérrez et al. suggested the DN reactions may proceed through the cooperation of the acidic $-SH$ species and their neighbouring basic S^{2-} ions.² Besides, only few studies thought not the acid site but the metal site (CUS) contributes to the C-N bond cleavage through "capturing" the N-containing molecules to form intermediate cycloalkanoates.^{21, 24}

As discussed above, although it can be assured that the HYD is closely related to both CUS sites and brim sites, and the DN is probably associated with the $-SH$ groups, S^{2-} ions and even the CUS sites, extensive debates about the origin of the active sites in HDN catalysts still exist. Hence, a desired model catalyst for further understanding the origin should be urgently needed. However, the catalysts exploited present either belong to the far-unrealistic model catalysts, such as Au-loaded (Ni)MoS₂ nanoslabs under an ultrahigh vacuum condition used in STM studies mentioned above and the unsupported bulk phase ones,^{6, 17, 18} or are ascribed to the

conventional supported catalysts. The former strategy inevitably results in potentially inaccurate and even misleading research results unless certain precautions are taken into account. For the latter strategy, the traditional preparation route by sulfidation of oxidic precursors (generally MoO_x NPs) to yield sulfided catalysts makes it difficult to effectively adjust the microstructure and edge composition while avoiding the strong interference from the alumina support,^{6, 9, 10} which thereby brings the great difficulty to accurately understand the nature of the active sites of HDN catalysts.

Although the synthesis and structure characterizations of amorphous molybdenum trisulfide (MoS₃) with different morphologies have been continuously reported for several decades,²⁵⁻²⁸ until recently its uses as excellent hydrogen-generation catalysts and outstanding precursors of the MoS₂-based catalysts start to be paid more attention.²⁹⁻³⁵ To the best of our knowledge, however, no studies have been reported in the literature using MoS₃ NPs instead of the conventional MoO_x NPs as the precursor to prepare the desired model MoS₂/Al₂O₃ catalyst for understanding the origin of the active sites. In the previous study,³³ we reported a simple ethanol-assisted chemical deposition method to synthesize a MoS₃/Al₂O₃ composite, followed by a thermally treatment under H₂ atmosphere to yield a MoS₂/Al₂O₃ catalyst with excellent DBT HDS activity. Based on this discovery and the further improvement, herein we propose a novel strategy to fabricate three MoS₂/Al₂O₃ catalysts with controlled MoS₂ nanosize, tunable edge composition and Ni-promoting effect in the absence of strong metal-support interaction by using the as-synthesized alumina-supported MoS₃ NPs as a precursor, as shown in Scheme 1. In our approach, the MoS₃ NPs were first loaded onto the surface of γ -Al₂O₃ by a simple chemical deposition method and then thermally treated under atmosphere H₂, N₂ and H₂S, respectively, to obtain three MoS₂/Al₂O₃ catalysts with the same nanosize of MoS₂ NPs but different S/Mo atom ratios while avoiding the strong interference to the metal phase from the alumina support. Then the effects of edge composition on the HDN performance and Ni-promoting effect and thereby the origin of the active sites were thoroughly studied using the most representative



Scheme 1 Alumina-supported MoS₃ NPs were first synthesized by chemical deposition method and then used as the precursor to prepare MoS₂/Al₂O₃ catalysts with controlled MoS₂ nanosize, tunable edge composition and Ni-promoting effect.

quinoline (Q) as the model reactant.

Experimental

Synthesis of alumina-supported MoS₃ NPs

A typical synthesis procedure of the alumina-supported MoS₃ NPs is described as follows: first, about 4.5 mL of a 2.4 M HCl solution was added into 15.5 mL of a solution containing 1.44 g thioacetamide (CH₃CSNH₂, TAA, AR, supplied by Sinopharm Chemical Reagent Co., Ltd, P. R. China) and 1.45 g sodium molybdate (Na₂MoO₄·2H₂O, AR, supplied by Sinopharm Chemical Reagent Co., Ltd, P. R. China) under stirring to yield 20 mL of an acid solution with pH=4.5; then 40.0 mL anhydrous ethanol was added into the stirred acid solution and the resulting solution was transferred to a 100-ml rotary Teflon-lined stainless steel autoclave containing 4.0 g γ -Al₂O₃ extrudates (97.7% Al₂O₃, average diameter 1.5 mm, surface area 215 m²/g, pore volume 0.6 mL/g, supplied by Shandong Alumina Plant, P. R. China) and heated at 84 °C for 12 h; finally, the resulting alumina-supported MoS₃ NPs (also denoted as MoS₃/Al₂O₃ composite in the following) was filtered, washed with deionized water and anhydrous ethanol, respectively, and then dried at 100 °C in N₂ atmosphere for 4 h and later kept in the vacuum glove box for further use.

Specially, for clearly proving successful synthesis of alumina-supported MoS₃ NPs, a counterpart with bulk MoS₃ supported on the alumina was meanwhile prepared by the incipient wetness impregnation of γ -Al₂O₃ with a black emulsion-like suspension containing Molybdenum sulfide dihydrate (MoS₃·2H₂O, AR, supplied by Alta Aesar-A Johnson Matthey Company) at 90 °C, and then dried at 100 °C in N₂ atmosphere for 4 h and later kept in the vacuum glove box for further analysis. This counterpart is noted as "bulk-MoS₃/Al₂O₃".

Thermally treating MoS₃/Al₂O₃ composite to yield MoS₂/Al₂O₃ catalysts

This procedure was operated in a continuously flowing tubular fixed-bed microreactor of internal diameter 10.0 mm and length 500 mm and specific process is described as follows: first, quickly shift the as-synthesized MoS₃/Al₂O₃ composite from the vacuum glove box into the microreactor without exposing to the air as possible and on both sides of the composite some quartz particles of 0.90 mm in diameter are needed to support it in the constant temperature zone of the reactor; then, the composite is treated in H₂, N₂ and H₂S/Ar (10 vol.%) at 500 °C for 4 h with gas flow rate of 300 mL/min and total pressure of 4.0 MPa, respectively, to yield three MoS₂/Al₂O₃ catalysts, which are noted as PSH-CAT, PSN-CAT and PSS-CAT, correspondingly. The catalysts are crushed and sieved to uniform particles (40-60 mesh in size) in the vacuum glove box, and then kept in vacuum for further use. The comparative MoO₃ loading in the three sulfided catalysts determined by X-ray fluorescence spectroscopy (XRF, Rigaku ZSX-100e) was about 14.5 wt%.

For fully demonstrating the advantages of using MoS₃ NPs as the precursor instead of the conventional MoO_x NPs, a

conventional sulfided MoS₂/Al₂O₃ catalyst with the identical Mo content was prepared according to the following procedure: first, alumina-supported MoO_x NPs (noted as MoO_x/Al₂O₃ composite) were prepared by the incipient wetness impregnation of γ -Al₂O₃ extrudates with an aqueous solution of ammonium molybdate and ammonia, and afterward drying at 120 °C for 2 h and calcination at 500 °C for 4 h in air; then MoO_x/Al₂O₃ was sulfided in the fixed-bed microreactor mentioned above with a mixture of 3wt% CS₂ in cyclohexane at a temperature of 360 °C for 4 h with liquid hourly space velocity (LHSV) of 20 h⁻¹, total pressure of 4.0 MPa, and H₂/hydrocarbon volumetric ratio of 500, to yield the MoS₂/Al₂O₃ catalyst, noted as IM-CAT. The comparative MoO₃ loading determined by XRF was 14.3%, which are nearly equal to the above three sulfided catalysts.

Preparation of Ni-decorated MoS₂/Al₂O₃ bimetallic catalysts

The typical procedure of introducing Ni onto the MoS₂/Al₂O₃ catalyst is shown as follows: three Ni-MoS₂/Al₂O₃ bimetallic catalysts noted as Ni-PSH-CAT, Ni-PSN-CAT and Ni-PSS-CAT were prepared by the incipient wetness impregnation of PSH-CAT, PSN-CAT and PSS-CAT with an aqueous solution of Ni(CH₃COO)₂ with the molar ratio of Ni to Mo at 3:7, respectively; after impregnation, the solids were dried at 120 °C for 2 h in a N₂ atmosphere and thermally treated at 500 °C for 4 h in a 15 vol.% H₂S/H₂ atmosphere. The comparative MoO₃ and NiO contents in the three bimetallic catalysts determined by XRF were 14.3 wt% and 3.2 wt%, respectively.

Characterizations of the composite precursor and the sulfided catalyst

X-ray photoelectron spectroscopy (XPS) studies were carried out on a VG Scientific ESCALab 220i-XL spectrometer using Al K α radiation. The analyzed procedures are described as follows. First, the samples were cooled to room temperature in a nitrogen flow, and kept in cyclohexane to prevent oxidation. Before the measurement, the samples were pressed onto a stainless steel sample holder and then immediately mounted onto the XPS machine. Quantification of the surface contents of the elements was operated using the sensitivity factors provided with the VG software. For distinguishing the chemical state of the molybdenum species and also quantifying the contents of Mo⁴⁺, Mo⁵⁺ and Mo⁶⁺ species, the resulting XPS spectra were fitted using XPSPEAK software (Version 4.1)³⁶. For accurately testing the S/Mo atom ratio, XPS analysis combined with plasma-coupled atomic emission spectroscopy (AES-ICP) was carried out to obtain the Mo content and a Strohlein Instruments CS-MAT 5500 analyzer was operated to obtain the S content.

XRD analysis was operated on a Philips X'Pert diffractometer equipped with Cu K α radiation (wavelength 1.5406 Å), and the patterns were collected in the 2 θ range between 5° and 70° with a scanning speed of 2°/min. It is worthy to note that, for avoiding the phase transformation due to the oxidation by the air, the samples MoS₃/Al₂O₃ and bulk-MoS₃/Al₂O₃ should be shifted from the glove box to the apparatus as soon as possible.

N₂ adsorption-desorption measurements of the supports and corresponding catalysts were carried out on a Micromeritics ASAP 2002 instrument. The samples were first degassed under a vacuum of 10⁻⁵ Torr for 15 h at 250 °C, and then analyzed at liquid nitrogen temperature. Brunauer-Emmett-Teller (BET) and Barret-Joyner-Halenda (BJH) methods were used to calculate the specific surface areas and the average pore size, respectively. From the N₂ adsorption-desorption isotherms, the pore volumes of the samples could be calculated.

High-resolution transmission electron microscopy (HRTEM) were operated on a Philips Tecnai G2 F20 instrument, with an electron energy of 200 keV, Cs = 0.5 mm, a point-to-point resolution of 1.9 Å in TEM mode, and specimen tilt ±40°. The images were recorded on a TVIPS 1k×1k CCD camera. For quantitatively learning the metal sulfide slabs on the three sulfided catalysts, the lengths and stacking layer numbers of 300~500 MoS₂ nanoslabs from at least 30 representative micrographs obtained from different parts of one catalyst were measured. The average slab length (\bar{L}) and stacking layer number (\bar{N}) were calculated according to the following formula:¹⁰

$$\bar{L}(\bar{N}) = \frac{\sum_{i=1}^n x_i M_i}{\sum_{i=1}^n x_i} \quad (1)$$

where M_i is the slab length or stacking layer number of a MoS₂ nanoslab, and x_i is the number of slabs or stacks in a given range of lengths or stacking layer numbers.

In some studies, the MoS₂ dispersion was often calculated by dividing the total number of Mo atoms located at the edge surface by the total number of Mo atoms. Hence, in this article the value of equation (2) (denoted by f_{Mo}) is also used to express the MoS₂ dispersion on the support.^{10, 37}

$$f_{\text{Mo}} = \frac{M_{\text{Oedge}}}{M_{\text{Ototal}}} = \frac{\sum_{i=1}^t (6n_i - 6)}{\sum_{i=1}^t (3n_i^2 - 3n_i + 1)} \quad (2)$$

where n_i is the number of Mo atoms along one edge of a MoS₂ slab determined from its length ($L = 3.2(2n_i - 1)$ Å), and t is the total number of slabs determined from HRTEM images of a sulfided catalyst. In our test, we chose $t = 400$.

Catalytic performance assessment

The catalytic activity of the three MoS₂/Al₂O₃ catalysts and three Ni-MoS₂/Al₂O₃ bimetallic catalysts was assessed in the fixed-bed microreactor mentioned above. 1 wt% dibenzothiophene (DBT) in heptane and 1 wt% Q in heptane were chosen as the model compounds, respectively. A 0.50 g sample of the catalyst to be assessed was diluted with quartz particles of 0.25 mm in diameter to a constant volume of 2.0 mL before being loaded into the reactor. The reactions were carried out under the conditions of 280-400 °C, liquid hourly space velocity (LHSV) 20 h⁻¹ or other values as specified, total pressure 4.0 MPa, and H₂/hydrocarbon volumetric ratio 500.

After a stabilization period of 4 h, the reaction products were collected every two hours and analyzed using an HP 6890 gas chromatograph (GC) installed with a flame ionization detector and a 0.25 mm × 100 m dimethylpolysiloxane capillary column.

Assuming a pseudo-first-order reaction for both DBT HDS and Q HDN, the HDS and HDN reaction activity (noted as $K_{\text{HDS(N)}}$) of the catalysts were expressed by the following equation:⁶

$$K_{\text{HDS(N)}} = \frac{F}{m\tau} \ln\left(\frac{1}{1-\tau}\right) \quad (3)$$

where F is the feeding rate of the reactant DBT or Q in mol s⁻¹, m is the catalyst mass in gram, and τ is the total conversion of DBT or Q, and K_{HDS} and K_{HDN} are the rate constants of HDS and HDN in mol g⁻¹ s⁻¹, respectively.

DBT is a representative sulfur-containing compound found in petroleum and its HDS reaction network on Mo-based catalysts accepted extensively, in which DBT HDS proceeds through two pathways:^{10, 38} one is the direct desulfurization (DDS) route to produce biphenyl (BP), and the another is the hydrogenation (HYD) route to yield cyclohexylbenzene (CHB) and little dicyclohexyl (DCH) with tetrahydrodibenzothiophene (THDBT) and hexahydrodibenzothiophene (HHDBT) as intermediates. Hence, the reaction rate constants for DDS route (k_{DDS}) and HYD route (k_{HYD}) can be expressed by the following two equations, respectively:

$$k_{\text{DDS}} = K_{\text{HDS}} \times S_{\text{BP}} \quad (4)$$

$$k_{\text{HYD}} = K_{\text{HDS}} \times S_{\text{CHB+DCH}} \quad (5)$$

where S_{BP} and $S_{\text{CHB+DCH}}$ represent the HDS product selectivity of route DDS and HYD, respectively and the sum of them is equal to the total HDS activity, expressed with k_{HDS} . It is worthy to note that k_{HDS} does not mean K_{HDS} , the latter means the total reaction rate, not only involving the desulfurization reactions, but also referring to the intermediate reactions.

Q was taken as the model reactant in this research and its HDN reaction scheme is proposed as shown in Fig.1. It is shown that Q-HDN proceeds mainly through two paths:^{2, 22, 39, 40} Path I Q→1,2,3,4-tetrahydroquinoline (14THQ)→*o*-propylaniline (OPA)→propylbenzene (PB) and Path II Q→14THQ/5,6,7,8-tetrahydroquinoline (58THQ)→DHQ→propylcyclohexylamine (PCHA)→PCHE (propylcyclohexene)→PCH (propylcyclohexane). Therein, due to the lower aromaticity than benzene ring, it is very easier for pyridine ring to proceed via a hydrogenation reaction and thereby the hydrogenation mainly proceeds via Q→14THQ, not Q→58THQ, however, 14THQ and 58THQ can transform from each other under certain conditions.^{2, 22, 39, 40} Specially, because it is almost impossible for PCHE→PB via the dehydrogenation reaction under conventional reaction conditions, the product selectivity ratio of $S_{\text{PCHE+PCH}}/S_{\text{PB}}$ could be used to assess the two paths' contribution to the total HDN activity. The denitrogenation activity of the two paths can be expressed by the two following equations, respectively.

$$k_I = K_{HDN} \times S_{PB} \quad (6)$$

$$k_{II} = K_{HDN} \times S_{PCHE+PCH} \quad (7)$$

where S_{PB} and $S_{PCHE+PCH}$ represent the denitrogenation product selectivity of Path I and Path II, respectively, and the sum of them is equal to the total denitrogenation activity, noted as k_{HDN} . It is also worthy to note that k_{HDN} does not mean K_{HDN} , the latter means the total reaction rate, not only involving the denitrogenation reactions, but also referring to the intermediate reactions.

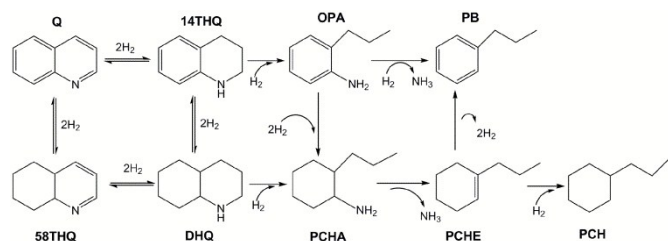


Fig. 1. Q HDN reaction network on (Ni)MoS₂/Al₂O₃ catalysts.

Results and discussion

Characterization results of alumina-supported MoS₃ nanoparticles

For demonstrating the as-deposited material ascribed to MoS₃, XPS analysis was first carried out. Fig. 2a shows the XPS survey spectra of γ -Al₂O₃ and MoS₃/Al₂O₃ composite. It can be clearly seen that, except for the characteristics of γ -Al₂O₃ and one peak of C1s from the adventitious impurity, the survey spectrum of MoS₃/Al₂O₃ shows predominantly peaks from Mo and S, and the peaks at 163.5, 231.3, 396.0 and 413.3 eV are ascribed to S2p, Mo3d, Mo3p_{3/2} and Mo3p_{1/2}, respectively.⁴¹ For further confirming the Mo species, the Mo3d and S2p spectra are further analyzed by fitting their curves, as shown in Fig. 2b and 2c, respectively. The Mo3d region reveals a mixture of Mo oxidation states, and peak fitting shows that ~24.3% of the Mo signal corresponds to a +6 oxidation state and ~75.7% of the Mo signal arises from the molybdenum sulfide, which likely corresponds to a lower oxidation state of +4.²⁹ The S2p spectrum consists of two doublets with S2p_{2/3} energies of 162.0 and 163.3 eV. The relative intensity of the doublets is 5:4, favoring the doublet with a higher binding energy. The spectrum suggests the existence of both S²⁻ and S₂²⁻ ligands, which are consistent with previous reports of amorphous MoS₃ materials.^{29, 42} Besides a small peak observed near 169.0 eV corresponds to the binding energy of sulfur in a sulfate group and likely arises from residual SO₄²⁻ probably formed in the process of material synthesis. Especially, the amorphous structure for the as-synthesized alumina-supported MoS₃ material is well shown by TEM image, as shown in Fig. 5a below, in which no diffraction pattern was observed.⁴²

Besides, the XPS analysis in combination with AES-ICP and CS-MAT reveals that the S/Mo atom ratio in the material is equal to 2.89 (shown in Table 3 below), which closely matches that of MoS₃.²⁹ Thus, the atomic composition and binding

energies measured by XPS and the amorphous structure observed by TEM suggest that the as-deposited material is predominantly composed of amorphous MoS₃. It is worthy to note that, compared with the XPS survey spectrum of γ -Al₂O₃, the peaks of Al2p, Al1s and O1s do not shift, indicating that the deposition of MoS₃ species did not change the chemical state of the alumina surface and no strong interaction induced by chemical bonds existed between the MoS₃ species and γ -Al₂O₃,⁴³ thereby in favor of ensuring the MoS₃-derived catalysts to exhibit a weak metal-support interaction, as confirmed by the following XPS characterization results.

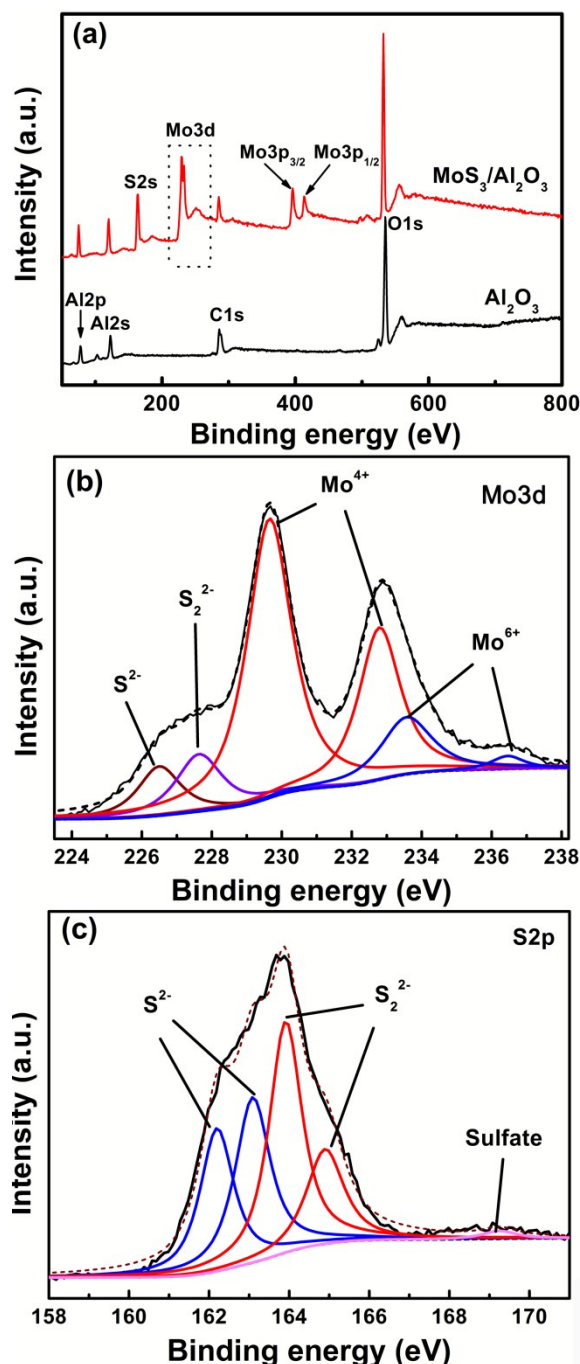


Fig. 2 (a) XPS survey spectra of γ -Al₂O₃ and MoS₃/Al₂O₃ composite; (b) the measured and curve-fitted Mo3d spectra of MoS₃/Al₂O₃ composite; and (c) the measured and curve-fitted S2p spectra of MoS₃/Al₂O₃ composite.

XRD analysis was then conducted to prove the successful synthesis of alumina-supported MoS₃ NPs, and the patterns of the samples γ -Al₂O₃ and MoS₃/Al₂O₃ were shown in Fig.3. For comparison purpose, both bulk-MoS₃/Al₂O₃ with bulk MoS₃ supported on the alumina surface which was prepared according to the method described in the Experimental Section and the pure MoS₃ material were meanwhile analyzed and the results were also shown in Fig.3. It can be clearly seen that MoS₃/Al₂O₃ exhibits the identical patterns with that of γ -Al₂O₃, but characteristic peak at about 14.4 ° of amorphous bulk MoS₃ or the pure MoS₃ material does not appear in the XRD pattern of MoS₃/Al₂O₃,⁴⁴ powerfully indicating that the as-deposited MoS₃ particles are too small to be detected by the XRD analysis.^{10, 45} It is extensively considered that the detectability of XRD analysis is about 4 nm,^{10, 45, 46} so the above results also imply no MoS₃ particle in MoS₃/Al₂O₃ is larger than 4 nm, which can be further confirmed by the following TEM images of the MoS₃-derived MoS₂/Al₂O₃ catalysts.

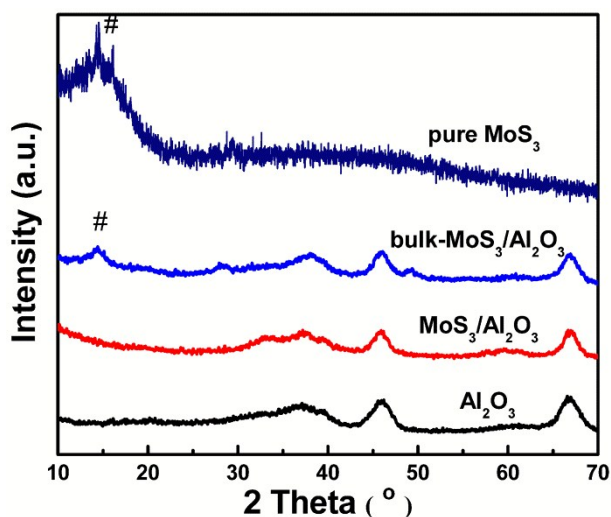


Fig. 3 XRD patterns of γ -Al₂O₃, MoS₃/Al₂O₃, bulk-MoS₃/Al₂O₃ and pure MoS₃ material.

The N₂ adsorption-desorption isotherms of the γ -Al₂O₃ and MoS₃/Al₂O₃ composite are shown in Fig. 4a, which are all type IV ones with a typical H2 type hysteresis loop and thus demonstrate the mesoporous characteristics of the solids. Fig. 4b shows that compared with that of γ -Al₂O₃, the pore size distribution of the MoS₃/Al₂O₃ composite becomes narrower and the most probable pore diameter decreases greatly from ca. 9.2 nm to ca. 7.5 nm. The textural properties of the two samples are listed in Table 1, which shows obvious losses in the specific surface areas (215 vs. 196 m² g⁻¹), pore volumes (0.60 vs. 0.51 mL g⁻¹), and average pore diameters (10.2 vs. 8.7 nm) after the incorporation of MoS₃ NPs into γ -Al₂O₃. The above results fully indicate that MoS₃ NPs have been successfully deposited into the pores of γ -Al₂O₃.^{10, 47}

It has been well proved that TAA will undergo slow hydrolysis to release H₂S in acidic condition at above 80 °C,^{33, 34} as expressed by Equation (8). The resulting H₂S molecules will immediately react with the surrounding MoO₄²⁻ anions and H⁺ cations to produce MoS₃ precipitate nanoparticles, as expressed by Equation (9). Then, the generated MoS₃

nanoparticles will continuously diffuse into the pores of alumina and deposit onto the pore surface to fabricate MoS₃/Al₂O₃ composite. Importantly, the electrostatic attraction between MoS₃ NPs with certain electronegativity originated from the “sulfur-rich” surface structure (can be easily proved by Zeta potential analysis, not shown here) and the protonated surface of alumina in the acidic synthesis system could be the primary cause of successful diffusion-deposition into the pores of γ -Al₂O₃.²⁵ Besides, except for acting as a dispersant to assist the deposition process as suggested by the previous study,³³ ethanol maybe play another important role, that is, the utilization of ethanol-water solution can create a “hydrothermal-like” condition at the used temperature 84 °C, because the bubble point temperature of the synthesis solution system is equal to about 81 °C. The hydrothermal deposition technology has been widely used for homogeneously diffusing-depositing nanoparticles with controllable size and shape onto the internal surface of porous substrates.^{10, 45, 46}

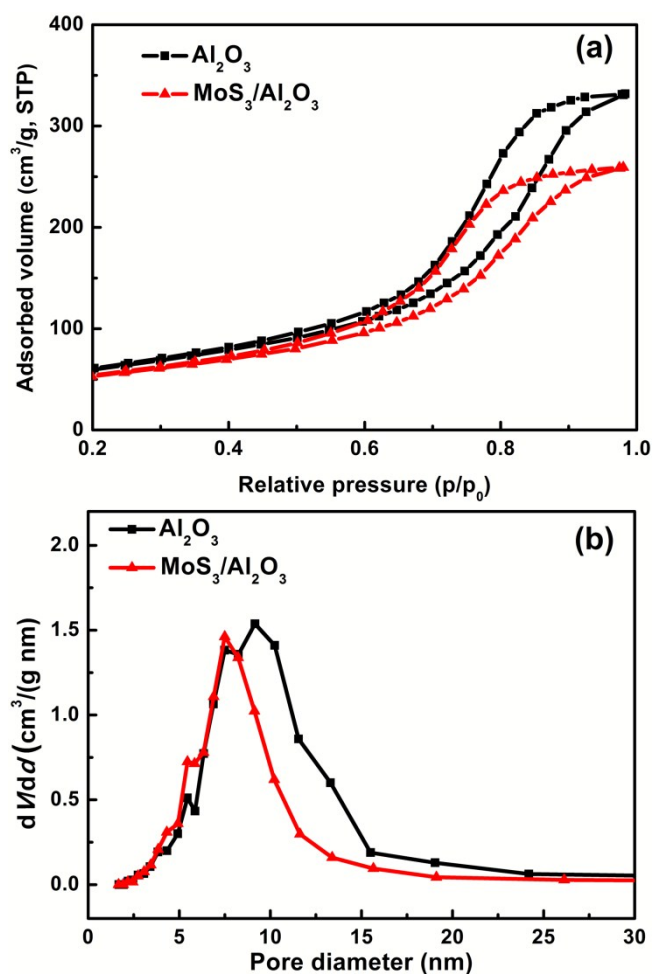
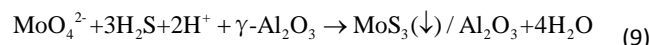


Fig. 4 N₂ adsorption-desorption isotherms (a) and BJH pore size distribution curves (b) of γ -Al₂O₃ and MoS₃/Al₂O₃

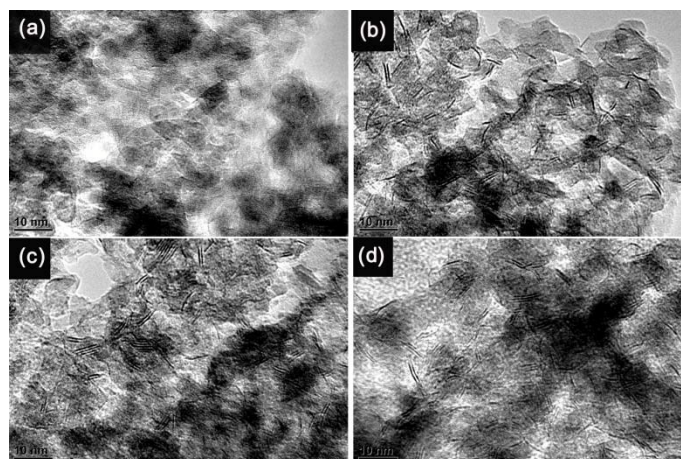
Table 1 Textural properties of γ -Al₂O₃ and MoS₃/Al₂O₃

Samples	S_g^a (m ² g ⁻¹)	V_p^b (cm ³ g ⁻¹)	D_p^c (nm)
γ -Al ₂ O ₃	215	0.60	10.2
MoS ₃ /Al ₂ O ₃	196	0.51	8.7

Notes: ^a BET surface area; ^b pore volume; ^c average pore diameter ($4V_p/S_g$).

Characterization results of MoS₃-derived MoS₂ catalysts

It is widely known that MoS₃ materials can decompose into MoS₂ compounds above 310 °C under the atmosphere of any non-oxidizing gas. A lot of studies about the activation process of conventional hydrotreating catalysts have pointed MoS₃ in fact is one of the intermediate states from MoO_x species to the final MoS₂ active particles.⁴⁸⁻⁵⁰ Fig. 5 shows the HRTEM images of MoS₃/ γ -Al₂O₃ composite and its-derived catalysts PSH-CAT, PSN-CAT and PSS-CAT which are prepared by thermal treatment under H₂, N₂ and H₂S atmospheres, respectively. Compared with the amorphous surface of MoS₃/Al₂O₃ composite as shown in Fig. 5a, its three derived catalysts all contain numerous dispersed MoS₂ nanocrystallites of uniform size with suitable stacking on the surface of alumina, as shown in Fig. 5b-5d. And the further analysis of the lamellar crystallites revealed that the interlamellar spacing of (002) was ca. 0.62 nm, indicating they are MoS₂ species.^{20, 51} The statistical calculation results from the HRTEM images of the three catalysts listed in Table 2 clearly show that, the average length, stacking and the edge-Mo dispersion of the MoS₂ nanoslabs of the three catalysts are nearly the same, effectively indicating that using MoS₃ NPs as the precursor can obtain series catalysts with controlled nanoparticle size of MoS₂. Moreover, from the average length of MoS₂ NPs below 4.0 nm, it is not difficult to infer that of the precursor MoS₃ NPs is also below the value, which is consistent with the above XRD result of MoS₃/Al₂O₃ composite. The N₂ adsorption-desorption characterization results of PSH-CAT, PSN-CAT and PSS-CAT are also listed in Table 2, which clearly shows that the three MoS₃-derived catalysts possess nearly the same textural properties. The above analysis demonstrates that using MoS₃ NPs instead of conventional MoO_x species as the precursor can obtain series catalysts with controlled micromorphology and textural properties.

**Fig. 5** Typical HRTEM images of MoS₃/ γ -Al₂O₃ composite (a) and its-derived catalysts: PSH-CAT (b), PSN-CAT (c) and PSS-CAT (d).**Table 2.** HRTEM and N₂ adsorption-desorption characterization results of PSH-CAT, PSN-CAT and PSS-CAT

Catalysts	MoS ₂ morphology parameters			Textural properties		
	\bar{L} (nm)	\bar{N}	f_{Mo}	S_g^a /m ² g ⁻¹	V_p^b /cm ³ g ⁻¹	D_p^c /nm
PSH-CAT	3.2	2.2	0.37	202	0.53	8.9
PSN-CAT	3.2	2.3	0.37	200	0.52	9.0
PSS-CAT	3.3	2.3	0.36	201	0.53	8.9

Notes: ^a BET surface area; ^b pore volume; ^c average pore diameter ($4V_p/S_g$). These results clearly demonstrate that using MoS₃ NPs instead of conventional MoO_x species as the precursor can obtain series catalysts with controlled micromorphology and textural properties.

For obtaining the information about the oxidation state and sulfidation degree of the Mo species, and meanwhile learning the metal-support interaction intensity, the Mo3d and S2p XPS spectra of the three MoS₃-derived catalysts PSH-CAT, PSN-CAT, PSS-CAT together with the conventional catalyst IM-CAT were measured and systematically deconvoluted, and the results are shown in Fig. 6 and Fig. 7, respectively. The binding energies of the Mo3d_{5/2} and Mo3d_{3/2} levels for Mo⁴⁺ (MoS₂) are about 228.98 and 232.13 eV, those for Mo⁵⁺ (MoO_xS_y) are about 230.40 and 233.60 eV, those for Mo⁶⁺ (MoO₃) are about 232.51 and 235.71 eV and that for the S2s level are about 226.2 eV.⁴³ The binding energies of the S2p_{3/2} and S2p_{1/2} levels for S²⁻ (MoS₂) are about 162.30 and 163.48 eV and those for S²⁻ (MoO_xS_y) are about 163.50 and 164.68 eV.⁴³ Besides, the S2p spectra of S²⁻ (sulfate) was deconvoluted as a s orbital with the binding energy of 169.0 eV. The results clearly show that, obviously different from the Mo3d and S2p spectra of IM-CAT showing characteristics of MoS₂, MoO_xS_y and MoO₃ species, those of the MoS₃-derived catalysts exhibit almost the same curves with predominant characteristics peaks of MoS₂ species. The sulfidation degree of molybdenum species in catalysts, denoted as Mo_{sulfidation}, is defined as the ratio of Mo⁴⁺ (MoS₂) to the sum of Mo⁴⁺ (MoS₂), Mo⁵⁺ (MoO_xS_y) and Mo⁶⁺ (MoO₃), i.e., $Mo_{sulfidation} = Mo^{4+} / (Mo^{4+} + Mo^{5+} + Mo^{6+})$.¹⁰ The fitting

ARTICLE

results in Table 3 show that $\text{Mo}_{\text{sulfidation}}$ of the three MoS_3 -derived catalysts are all near to 100%, much higher than that of the conventional catalyst IM-CAT ($\text{Mo}_{\text{sulfidation}}=65.8\%$).

The above results powerfully illustrate that using MoS_3 NPs instead of the conventional MoO_x NPs can promote the Mo sulfidation to maximum. Moreover, because the sulfidation degree reflects the metal-support interaction, the nearly full-sulfidation also signifies the MoS_3 -derived catalysts present no strong metal-support interaction, whereas which often exists in the conventional catalysts.^{45, 46} In other word, using alumina-supported MoS_3 NPs as the precursor can effectively avoid the strong interference to the metal phase from the alumina support. In addition, the full-sulfidation or weak metal-support interaction of the three catalysts also imply that the active sites are overwhelming the widely-agreed "type II" ones which exhibits excellent intrinsic activity.^{46, 52} The resulting high catalytic activity was demonstrated by the HDS and HDN assessment results shown in Fig. S1 (See the Supporting Information), that is, the three MoS_3 -derived catalysts all exhibit much higher DBT-HDS and Q-HDN activity than those of the conventional catalyst IM-CAT.

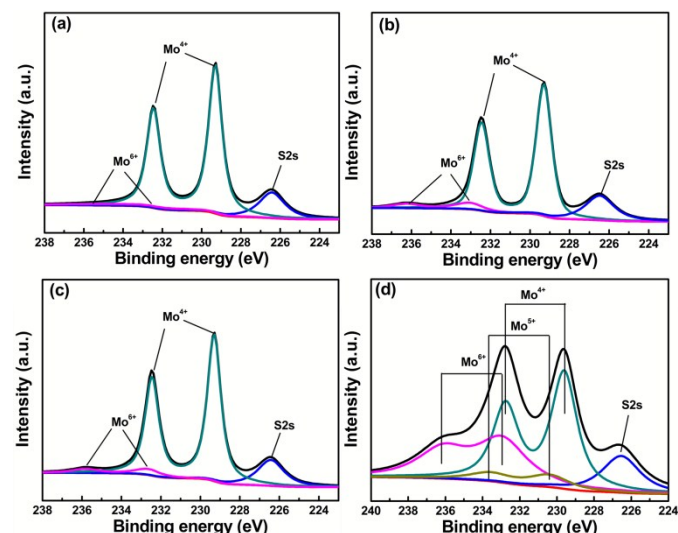


Fig. 6 The measured and curve-fitted Mo3d XPS spectra of PSH-CAT (a), PSN-CAT (b), PSS-CAT (c) prepared using MoS_3 as the precursor and conventional IM-CAT (d) prepared using MoO_x as the precursor.

Catalysis Science & Technology

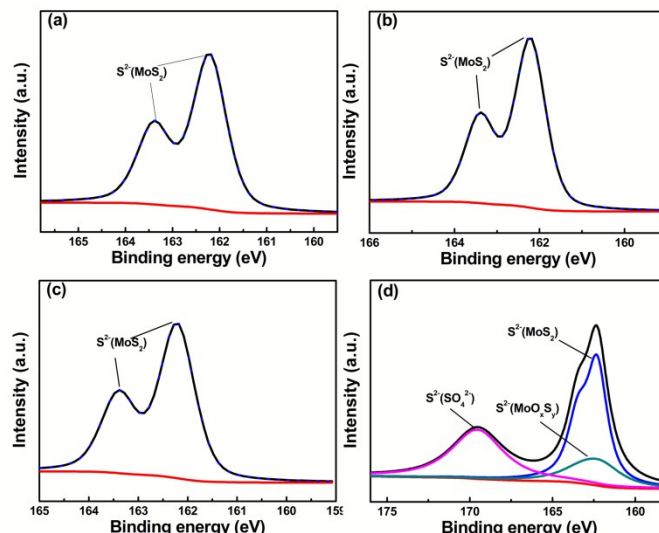


Fig. 7 The measured and curve-fitted S2p XPS spectra of PSH-CAT (a), PSN-CAT (b), PSS-CAT (c) prepared using MoS_3 as the precursor and conventional IM-CAT (d) prepared using MoO_x as the precursor.

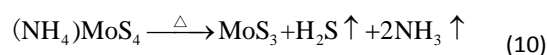
Table 3 XPS characterization results of the samples

Samples	Atmosphere	$\text{Mo}_{\text{sulfidation}}$ (%)	S/Mo*
$\text{MoS}_3/\text{Al}_2\text{O}_3$	-	75.3	2.89
PSH-CAT	H_2	99.3	1.61
PSN-CAT	N_2	98.8	1.95
PSS-CAT	H_2S	98.6	2.13
IM-CAT	H_2S	65.8	1.77

Note: *Obtained by XPS analysis in combination with AES-ICP and CS-MAT.

In recent years, for achieving hydrotreating catalysts containing more Type II active sites thereby with excellent performance, some studies have attempted to prepare unsupported $\text{Mo(W)}\text{S}_2$ based catalysts by the high-temperature pyrolysis of thiomolybdate or thiotungstate salts,⁵³⁻⁵⁵ taking ammonium tetrathiomolybdate for an example, as shown in the following Equation (10). These studies agreed that, before the transformation of these salts into MoS_2 active phase, these salts must first undergo their decomposition into MoS_3 -like species. Later, a few studies observed that, by shifting the atmosphere used in the thermal treatment process, the microstructure and composition of the active phase could be effectively modified.^{56, 57} Okamoto et al. studied the influence of two sulfidation atmospheres (10 vol.% $\text{H}_2\text{S}/\text{H}_2$ vs. 10 vol.% $\text{H}_2\text{S}/\text{He}$) on the local structure and intrinsic activity of the Co-Mo-S phase and found that⁵⁶, compared with $\text{H}_2\text{S}/\text{H}_2$ atmosphere, $\text{H}_2\text{S}/\text{He}$ atmosphere not only promotes a higher Mo-edge/S-edge ratio, but also facilitates the formation of local structure including a dinuclear Co sulfide cluster with a sulfur dimer between the two Co atoms, which further increases the intrinsic activity of the resulting catalyst. Afanasiev prepared series unsupported MoS_2 catalysts by thermally decomposing ammonium tetrathiomolybdate, and

studied the influence of two atmospheres (pure H₂ and pure H₂S gases) on the microstructure and composition of the active phase.⁵⁷ Results showed that, the different treatment atmospheres directly led to the difference composition and structure of the active phase edge, that is, when treated with H₂S, the S/Mo atom ratio is above 2 and some S₂²⁻ groups were created on the edge, and these groups are supposed to easily react with the activated hydrogen to form -SH sites, thus facilitating the HYD reaction of thiophene; when treated with H₂, the S/Mo atom ratio is below 2, and there is no S₂²⁻ group but some CUS sites on the edge, thereof in favor of the DDS reaction of thiophene. Meanwhile they emphasized that, the conclusions are only suitable for HDS reactions. Whereas for the hydrogenation reactions of non-sulfur molecules, the created CUS sites also greatly contribute to the hydrogenation activity.



Just inspired by the above studies, the as-synthesized MoS₃/Al₂O₃ composite with MoS₃ NPs loaded on the surface of alumina were thermally treated in H₂, N₂ and H₂S, respectively. The composition analysis results obtained in combination of XPS, AES-ICP and CS-MAT characterizations are listed in Table 3. It can be clearly seen that the consistent research results with those suggested by Afanasiev were obtained:⁵⁷ when treated with H₂, S/Mo=1.61, obviously under the stoichiometric ratio of 2; when treated with N₂, S/Mo=1.95, somewhat less than the stoichiometric ratio; when treated with H₂S, S/Mo=2.13, more than the stoichiometric ratio. It is very worthy to note that, just because of the nearly full sulfidation of the Mo species into MoS₂ active phase as discussed above, the above S/Mo ratios then could directly represent the edge-structure and edge-composition of the MoS₂ active phase. Hence, for conventional catalyst IM-CAT, due to the much lower sulfidation degree (65.8%), the S/Mo value of it means nothing. Therefore, catalyst PSH-CAT with the lowest S/Mo ratio exhibits a "sulfur-deficient" edge-structure with a higher proportion of CUS sites, while PSS-CAT with the highest S/Mo ratio holds a "sulfur-rich" edge structure with a higher proportion of S₂²⁻/-SH groups. The above analysis clearly shows another big superiority of using alumina-supported MoS₃ NPs as the precursor: effectively modify the edge composition of the MoS₂ active phase. However, unfortunately for utilizing the conventional MoO_x NPs as the precursor, due to the single activation strategy (using various sulfurizing reagent, such as CS₂), it is scarcely possible to modify the edge composition.⁴⁹

The above characterization results show three main superiorities originating from the switch of the precursor from the conventional MoO_x NPs to MoS₃ NPs: (i) can obtain series catalysts with controlled micromorphology and textural properties; (ii) can effectively avoid the strong interference to the metal phase from the alumina support; (iii) can effectively modify the edge composition of the MoS₂ active phase. These superiorities lay the foundation of accurately understanding the origin of the active sites for HDN reactions.

Effect of the edge composition of MoS₂ active phase on HDN performance

It should be first emphasized that, due to the current research on the HDS mechanism of DBT has been made more consensus,^{6, 10, 58} so to a certain extent, DBT can be used as a probe molecule for studying the "structure-function" relation and thereof the origin of active sites for HDN reactions. In this study, DBT and Q were used as the model reactants to assess the HDS and HDN catalytic activities of the three MoS₃-derived catalysts PSH-CAT, PSN-CAT and PSS-CAT, respectively.

HDS activity of DBT

Fig. 8 describes the product selectivity ratio of $S_{BP}/S_{CHB+DCH}$ on the three catalysts as a function of the reaction temperature. It can be concluded that, although increasing the temperature can exponentially enhance the conversion of DBT (which has been extensively proved,^{10, 58} not shown here), it hardly influences the $S_{BP}/S_{CHB+DCH}$ ratio. As introduced in Experimental Section, the selectivity of BP (S_{BP}) and CHB+DCH ($S_{CHB+DCH}$) can be used to express the selectivity of reaction path DDS and HYD, respectively. Hence, the $S_{BP}/S_{CHB+DCH}$ ratio shown in Fig. 8 is actually equivalent to the path selectivity ratio, noted as DDS/HYD. The above results clearly show that, the less of the S/Mo ratio, the more of DDS/HYD, especially when S/Mo=1.61, the contribution of DDS path to the total HDS activity is 6 times larger than that of HYD path, and on the contrary, when S/Mo=2.13, HDS mainly proceeds by the HYD path. For evaluating the influence of edge composition (S/Mo ratio) on the total HDS activity, DDS activity and HYD activity, respectively, the reaction rate constant k_{HDS} , k_{DDS} and k_{HYD} of the three catalysts with different S/Mo ratios were calculated, as listed in Table 4. With the S/Mo ratio increasing from 1.61 to 2.13, the k_{DDS} sharply decreases from $7.3 \times 10^{-8} \text{ mol} \cdot \text{g}^{-1} \cdot \text{s}^{-1}$ to $2.1 \times 10^{-8} \text{ mol} \cdot \text{g}^{-1} \cdot \text{s}^{-1}$, whereas the k_{HYD} increases from $1.0 \times 10^{-8} \text{ mol} \cdot \text{g}^{-1} \cdot \text{s}^{-1}$ to $2.6 \times 10^{-8} \text{ mol} \cdot \text{g}^{-1} \cdot \text{s}^{-1}$, when the total k_{HDS} varies from $8.3 \times 10^{-8} \text{ mol} \cdot \text{g}^{-1} \cdot \text{s}^{-1}$ to $4.7 \times 10^{-8} \text{ mol} \cdot \text{g}^{-1} \cdot \text{s}^{-1}$, in accordance with the variation tendency of k_{DDS} .

Plenty of studies show that the S/Mo ratio of the pure MoS₂ nanocrystallines can directly imply the edge composition and local structure,^{13, 16, 17} a higher S/Mo ratio means a higher proportion of S₂²⁻/-SH groups on the edge sites, and a lower S/Mo ratio implies relatively more CUS located on the edge sites.^{56, 57} Base on this, the above activity and selectivity results of DBT HDS fully indicate CUS acts as the active site for DDS, and the S₂²⁻/-SH groups (maybe including very few S₂²⁻ as previous reported⁵⁶) are very closed with the active sites for HYD. According to the current acknowledge about the HYD active sites in the HDS process, because of the remarkable metallic character and thereby the excellent activation capacity of hydrogen, the special brim site along the Mo-edge with a coordinatively saturated state can function as the active site for HYD,¹⁶⁻¹⁸ and the neighbouring S₂²⁻/-SH groups located on the edge can further strengthen the metallic character and enhance the HYD activity,^{16, 17} which can be used to reasonably explain the above results: with the increase of S/Mo ratio, the k_{HYD} increases. Besides, the result that the contribution of DDS path to the total HDS activity obviously exceeds that of HYD

ARTICLE

path clearly implies the active site of DDS exhibits much higher intrinsic activity than that of HYD.

In fact, the above results have been attained wide acknowledgments and verifications, which in turn indicate that using alumina-supported MoS₃ NPs as the precursor can indeed effectively modify the edge composition and microstructure and thus powerfully supports the previous characterization results.

Catalysis Science & Technology

Table 4 HDS and HDN activity over PSH-CAT, PSN-CAT and PSS-CAT at 360 °C, 4 MPa.

Catalyst	S/Mo	$(10^{-8} \text{ mol} \cdot \text{g}^{-1} \cdot \text{s}^{-1})$						
		k_{HDS}	k_{HYD}	k_{DDS}	k_{HDN}	k_{I}	k_{II}	$k_{\text{II}}/k_{\text{I}}$
PSH-CAT	1.61	8.3	1.0	7.3	0.070	0.017	0.053	3.1
PSN-CAT	1.95	5.3	2.1	3.2	0.25	0.040	0.21	5.3
PSS-CAT	2.13	4.7	2.6	2.1	0.58	0.10	0.48	4.8

Notes: k_{HDS} and k_{HDN} are the total desulfurization reaction rate constant and total denitrogenation reaction rate constant, respectively; k_{DDS} and k_{HYD} represent the desulfurization activity of DDS path and HYD path, respectively; k_{I} and k_{II} are the denitrogenation reaction rate constant of Path I (Q→14THQ→OPA→PB) and Path II (Q→14THQ(58THQ)→DHQ→PCHA→PCHE→PCH), respectively.

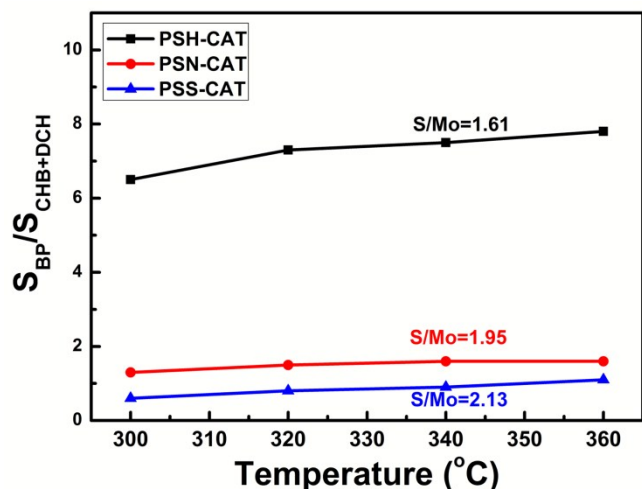


Fig. 8 Product selectivity ratio of BP/(CHB+DCH) on PSH-CAT, PSN-CAT and PSS-CAT as a function of the reaction temperature.

HDN activity of Q

Due to the molecular structure of Q, all reactions that take place in an industrial HDN process also occur in the HDN network of Q (shown in Fig. 1), that is, C-N bond cleavage, hydrogenation of aromatic heterocyclic rings, and hydrogenation of benzenic rings. Hence, Q was taken as the model reactant in this research. As mentioned previously, the HDN of Q proceeds through two paths:³ Path I Q→14THQ→OPA→PB and Path II Q→14THQ(58THQ)→DHQ→PCHA→PCHE→PCH. For assessing the respective contribution of the two paths to the total HDN activity, the k_{HDN} , k_{I} , k_{II} and $k_{\text{II}}/k_{\text{I}}$ ratio at 360 °C were measured, respectively, and the results are listed in Table 4. It can be clearly seen that with S/Mo ratio increasing from 1.61 to 2.13, k_{II} increases sharply from $0.053 \times 10^{-8} \text{ mol} \cdot \text{g}^{-1} \cdot \text{s}^{-1}$ to $0.48 \times 10^{-8} \text{ mol} \cdot \text{g}^{-1} \cdot \text{s}^{-1}$, and k_{I} increase substantially from $0.017 \times 10^{-8} \text{ mol} \cdot \text{g}^{-1} \cdot \text{s}^{-1}$ to $0.10 \times 10^{-8} \text{ mol} \cdot \text{g}^{-1} \cdot \text{s}^{-1}$, demonstrating that catalyst PSS-CAT with the “sulfur-richest” structure exhibits the highest catalytic activity of C-N cleavage and thus indicating that the DN active sites are very closed with the S²⁻/-SH groups. In addition, it is clear that k_{II} undergoes a more significant amplification than k_{I} , and thereby makes more contributions to the total HDN activity, which has been explained by some studies:^{4, 22} the intermediate hydrogenation product DHQ in Path II presents stronger adsorption ability to the active sites.

For further logically assessing the HYD and DN activities and then accurately understanding the nature of the active sites, the selectivity of HYD intermediate products (14THQ+58THQ+DHQ) and the selectivity of C-N bond cleavage (DN) products (OPA+PCHA+C9) on the three catalysts PSH-CAT, PSN-CAT and PSS-CAT at 360 °C were also compared with each other, and the results are listed in Table 5. Here “C9” expresses all the non-nitrogen containing products, e.g. PCHE, PB and PCH. It is noteworthy that, consistent with the most studies,^{22, 39} no PCHA and DHQ in the products were detected, mainly due to their high reactivity. Results shown in Table 5 demonstrate that with the S/Mo ratio increasing, the selectivity of HYD products thereupon decreases dramatically (from 88.4% to 64.6%), whereas that of DN products increases significantly (from 11.5% to 34.9%), fully indicating that the active sites of Q-HYD are very related to the CUS sites, and that of Q-DN are closely associated with the S²⁻/-SH groups. By further analysis, it can be found that the variation of S/Mo ratio only influences the HYD activity of Q→14THQ, but has no affect on that of Q→58THQ, suggesting that these two HYD reactions require different active sites, the former probably proceed on CUS sites, and the latter may take place on the brim sites, which needs further research. Moreover, according to the chemical reaction characteristics,^{1, 6} compared with 14THQ, 58THQ is more inclined to proceed HYD than 14THQ, because it bears obvious weaker thermodynamic equilibrium limit at higher reaction temperature, as detailedly demonstrated by the results shown in Fig. S2 (See the Supporting Information). Hence, enhancing the temperature is more beneficial to Q→58THQ→DHQ→PCHA→PCHE→PCH in Path II.

Table 5 HDN product selectivity over catalysts PSH-CAT, PSN-CAT and PSS-CAT at 360 °C, 4 MPa.

Catalyst	S/Mo	Q HDN product selectivity (%)					
		HYD products (14THQ+58THQ)			DN products (C9+OPA)		
		14THQ	58THQ	Total	C9	OPA	Total
PSH-CAT	1.61	68.4	20	88.4	4.4	7.1	11.5
PSN-CAT	1.95	48.7	19.6	68.3	15.1	16.5	31.6
PSS-CAT	2.13	45.4	19.2	64.6	17.6	17.3	34.9

Note: C9 expresses all the non-nitrogen containing products, e.g. PCHE, PB and PCH. The conversions were controlled nearly the same by modifying the feeding rate when needed.

Further analysis of the combined results of HDN activity and product selectivity shows that, the ring-open reaction of 14THQ→OPA is the rate-determining step of Path I, while the ring-hydrogenation reaction of 14THQ(58THQ)→DHQ is the rate-determining step of Path II, which is well consistent with the research results gained by Farag et al.^{6, 58} Because of the much more contribution of Path II than Path I to HDN activity, efforts to improve the HYD activity of 14THQ(58THQ)→DHQ should be made to enhance the HDN activity of the monometallic MoS₂-based catalysts. To overcome the excessively strong adsorption capacity of DHQ onto the active sites maybe the key solution to promote the reactivity of 14THQ(58THQ)→DHQ.

Through the comprehensive analysis results of DBT-HDS and Q-HDN reactions, it can be concluded as follows. CUS not only act as the active sites of DBT-DDS reaction, but also exhibit catalytic activity of reaction Q→14THQ; the S²⁻/-SH groups one hand enhance the catalytic activity of DBT-HYD through adjusting the electron structure of the brim sites, another hand probably play the role of active sites of Q-DN. In other word, there indeed exists dual functional active sites on a HDN catalyst: one for HYD and another for DN.

Effect of the edge composition of MoS₂ active phase on Ni-promoting effect

It is widely accepted that the anchoring of the promoting atoms Ni or Co can exponentially enhance the intrinsic catalytic activity of the resulting bimetallic catalysts,^{52, 58, 59} and therefore in these years what is the promoting effect and how to optimize it have always been the most critical and core issues in the research and development area of hydrogenation catalysts research and development.^{10, 47} However, because the most of the early studies about the promoting effect focus on the catalytic reaction systems of HDS, the resulting theoretical knowledges are often unsuitable to be adapted to explain the “structure-function” relations of HDN catalysts. Hence, fundamental research about the promoting effect of Ni/Co on HDN activity should achieve more widespread attention and development. STM studies combined with DFT theory methods show that,^{17, 18} the promoter atoms such as Ni

and Co could selectively decorate the S-edge sites and then change the micromorphology, microstructure and composition of the edges and the electronic structure of the MoS₂ phase. On the other hand, the change of the edge composition certainly will result in the variation of the promoting effect. In this research, the three catalysts PSH-CAT, PSN-CAT and PSS-CAT with different edge compositions were first used as the “second support” of the promoter atom Ni to prepare the corresponding NiMo-bimetallic catalysts Ni-PSH-CAT, Ni-PSN-CAT and Ni-PSS-CAT, and then the Ni-promoting effect on HDN activity was studied.

Table 6 HDS and HDN selectivity over MoS₂/Al₂O₃ and Ni-MoS₂/Al₂O₃ catalysts.

Catalyst	S/Mo	Activity and selectivity analysis results (10 ⁻⁸ mol·g ⁻¹ ·s ⁻¹)				
		<i>k</i> _{H_{DN}}	<i>SF</i> _{H_{DN}}	<i>k</i> _I	<i>k</i> _{II}	<i>k</i> _{II} / <i>k</i> _I
PSH-CAT	1.61	0.070	/	0.017	0.053	3.12
Ni-PSH-CAT	/	2.49	35.6	0.32	2.17	6.84
PSN-CAT	1.95	0.25	/	0.040	0.21	5.25
Ni-PSN-CAT	/	2.18	8.7	0.34	1.84	5.47
PSS-CAT	2.13	0.58	/	0.10	0.48	4.80
Ni-PSS-CAT	/	2.09	3.6	0.35	1.74	5.03

Notes: *k*_{H_{DN}} is the total denitrogenation reaction rate constant; *SF*_{H_{DN}} is synergetic factor, which equals to *k*_{H_{DN}}(Ni-MoS₂)/*k*_{H_{DN}}(MoS₂); *k*_I and *k*_{II} are the denitrogenation reaction rate constant of path I (Q→14THQ→OPA→PB) and path II (Q→14THQ(58THQ)→DHQ→PCHA→PCHE+PCH), respectively. Reaction conditions: HDS, 320 °C, 4 MPa; HDN, 360 °C, 4 MPa, and the conversions were controlled by modifying the feeding rate when needed.

The HDN activity and selectivity results of the three monometallic and their corresponding bimetallic catalysts are listed in Table 6, respectively. The results clearly show that, regardless of the edge composition of MoS₂ phase, *k*_{H_{DN}} of the three monometallic catalysts all increase largely after the addition of promoter atom Ni, indicating the presence of the strong Ni-promoting effect on HDN activity. To further compare the Ni-promoting effect in the three bimetallic catalysts, the synergetic factor (*SF*), defined by *SF*_{H_{DN}}=*k*_{H_{DN}}(Ni-MoS₂)/*k*_{H_{DN}}(MoS₂), were estimated and the results are also shown in Table 6, respectively. It can be seen that with the increase of S/Mo atom ratio of the edge, the *SF*_{H_{DN}} decreases substantially from 35.6 to 3.6, fully demonstrating that the “sulfur-deficient” edge structure is more beneficial for Ni-promoting effect on HDN activity, which is well consistent with the results from Afanasiev’s study.⁵⁷ For assessing the Ni-promoting effect on the activity of the two paths, *k*_I, *k*_{II} and *k*_{II}/*k*_I ratio are also listed in Table 6, which clearly shows that, regardless of the S/Mo ratios, when any of the monometallic catalysts is promoted by Ni atoms, both *k*_I and *k*_{II} increase sharply, but *k*_{II}/*k*_I value undergoes a slight increase, implying

that the promoter Ni atoms can enhance the Path I and Path II with the nearly same extent.

Recent years, some studies have pointed that,^{56, 57, 60} the “sulfur-deficient” edge structure of MoS₂ nanocrystallines (with S/Mo below the stoichiometric ratio of 2) possesses more CUS sites and thus can accommodate more Ni atoms to form more Ni-Mo-S active sites with high intrinsic activity, which also has been proved by STM studies in the last few years. However, for the “sulfur-rich” edge structure of MoS₂ nanocrystallines (with S/Mo above the stoichiometric ratio of 2), because of the presence of relatively more S²⁻/S₂²⁻ groups and the weaker affinity between these groups and Ni²⁺, only when these groups first react with activated hydrogen to transform into -SH groups, the Ni²⁺ can then react with these resulting -SH groups to form Ni-Mo-S active sites, finally resulting in a poor promoting effect. Similarly, as previous discussed in this research, the edge composition and microstructure directly influence the promotion effect, and the “sulfur-deficient” edge structure is more beneficial for Ni promoter role.

So far, a large number of basic researches have been carried out to understand the origin of Ni-promoting effect,^{11, 17, 18} and two potential roles for Ni atoms have been suggested: on one hand, it is first embedded into the edge of MoS₂ nanocrystallines and then act as an electron donor to increase the electron cloud density of its adjacent Mo atom, resulting in a weakened Mo-S bond energy and an increased instability of Mo-coordinated S to yield a CUS site which is contributed to the HYD activity; on the other hand, it optimizes the interaction between the reactants and the active sites, promoting the more effective energy and electron transfer through π -electron system between Mo-edge sites and the reactants and thus favouring the HYD reactions. Most recently, based on the HDN reaction network of DHQ on MoS₂/Al₂O₃ catalyst and its Ni-promoted one, Gutiérrez et al. yielded a new suggestion about Ni-promoting effect on HDN activity,² that is, Ni atoms replace part of the Mo atoms on the edges, which on one hand activate hydrogen molecular to produce activated hydrogen which afterwards react with the S²⁻ species to form -SH species, and on the other hand act as “electron donor” to increase the electron cloud density of the neighboring basic S²⁻, and then these two effects together promote the cracking of the β -H bonds (e.g. enhance the DN activity) according to Hofmann elimination reaction mechanism. Considering the HDN activity assessment results in this study that, the decoration for Ni atoms into the “sulfur-deficient” edges of PSH-CAT not only greatly increases the activity of Path I (Q \rightarrow 14THQ \rightarrow OPA \rightarrow PB) and but also significantly enhances that of Path II (Q \rightarrow 14THQ/58THQ \rightarrow DHQ \rightarrow PCHA \rightarrow PCHE \rightarrow PCH), the above suggestions provided by Gutiérrez et al. maybe the reasonable explanations. For further proving this, comprehensive study on “structure-function” of the bimetallic catalysts should be carried out in the future.

Conclusions

In summary, this article proposes alumina-supported MoS₃ NPs as a precursor of model catalysts to study the origin of the active sites for HDN reactions. The MoS₃ NPs were first loaded onto the surface of γ -Al₂O₃ by a simple chemical deposition method and then thermally treated under atmosphere H₂, N₂ and H₂S, respectively, to obtain three MoS₂/Al₂O₃ catalysts. The systematic characterization results show that three main superiorities originating from the switch of the precursor from the conventional MoO_x NPs to MoS₃ NPs: (i) can obtain series catalysts with controlled micromorphology and textural properties; (ii) can effectively avoid the strong interference to the metal phase from the alumina support; (iii) can effectively modify the edge composition of the MoS₂ active phase. These superiorities lay the foundation of accurately understanding the origin of the active sites for HDN reactions.

Then the effects of edge composition and microstructure of MoS₂ phase in the series MoS₃-derived catalysts on the HDN performance and Ni-promoting effect were thoroughly studied using Q as the model compound and comprehensive results are obtained: (i) there exist two type active sites in MoS₂/Al₂O₃ catalysts, one for HYD which is directly related with both CUS and brim sites and another for DN which is greatly connected with the -SH/S²⁻ groups on the edge of the active phase; (ii) the edge composition of MoS₂ phase directly influences the promotion effect and the “sulfur-deficient” edge structure is more beneficial for Ni promotion role.

Due to the actual catalyst model first used, the viewpoints shown in this article exhibit valuable guiding significance for high-efficient HDN catalyst development. Considering the above superiorities of using the MoS₃-derived catalysts as the model catalyst, further fundamental researches, such as origin of Ni-promoting effect, support effect and nanosize effect are needed to be carried out as soon as possible.

Acknowledgements

We gratefully acknowledge the supports from the National Basic Research Program of China (grant 2012CB224802).

Notes and references

- 1 E. Furimsky and F. E. Massoth, *Catal. Rev.*, 2005, **47**, 297-489.
- 2 O. Y. Gutiérrez, S. Singh, E. Schachtl, J. Kim, E. Kondratieva, J. Hein and J. A. Lercher, *ACS Catal.*, 2014, **4**, 1487-1499.
- 3 R. Prins, *Adv. Catal.*, 2001, **46**, 399-464.
- 4 T. C. Ho, *Appl. Catal. A*, 2010, **378**, 52-58.
- 5 S. L. González-Cortés, S. Rugmini, T. Xiao, M. L. H. Green, S. M. Rodulfo-Baechler and F. E. Imbert, *Appl. Catal. A*, 2014, **475**, 270-281.
- 6 H. Farag, M. Kishida and H. Al-Megren, *Appl. Catal. A*, 2014, **469**, 173-182.
- 7 C. Song, *Catal. Today*, 2003, **86**, 211-263.
- 8 J. R. Katzer and R. Sivasubramanian, *Catal. Rev.*, 1979, **20**, 155-208.
- 9 M. Breyse, C. Geantet, P. Afanasiev, J. Blanchard and M. Vrinat, *Catal. Today*, 2008, **130**, 3-13.
- 10 W. Han, P. Yuan, Y. Fan, G. Shi, H. Liu, D. Bai and X. Bao, *J. Mater. Chem.*, 2012, **22**, 25340-25353.

- 11 H. Topsøe, B. Clausen and F. Massoth, *Hydrotreating Catal. Sci. Tech.*, 1996, book.
- 12 M. Jian and R. Prins, *Catal. Today*, 1996, **30**, 127-134.
- 13 F. Besenbacher, M. Brorson, B. S. Clausen, S. Helveg, B. Hinnemann, J. Kibsgaard, J. V. Lauritsen, P. G. Moses, J. K. Nørskov and H. Topsøe, *Catal. Today*, 2008, **130**, 86-96.
- 14 B. Temel, A. K. Tuxen, J. Kibsgaard, N.-Y. Topsøe, B. Hinnemann, K. G. Knudsen, H. Topsøe, J. V. Lauritsen and F. Besenbacher, *J. Catal.*, 2010, **271**, 280-289.
- 15 J. V. Lauritsen, M. Nyberg, J. K. Nørskov, B. S. Clausen, H. Topsøe, E. Lægsgaard and F. Besenbacher, *J. Catal.*, 2004, **224**, 94-106.
- 16 H. Topsøe, B. Hinnemann, J. K. Nørskov, J. V. Lauritsen, F. Besenbacher, P. L. Hansen, G. Hytoft, R. G. Egeberg and K. G. Knudsen, *Catal. Today*, 2005, **107-108**, 12-22.
- 17 H. Topsøe, *Appl. Catal. A*, 2007, **322**, 3-8.
- 18 J. V. Lauritsen, J. Kibsgaard, G. H. Olesen, P. G. Moses, B. Hinnemann, S. Helveg, J. K. Nørskov, B. S. Clausen, H. Topsøe, E. Lægsgaard and F. Besenbacher, *J. Catal.*, 2007, **249**, 220-233.
- 19 L. Qu and R. Prins, *Appl. Catal. A*, 2003, **250**, 105-115.
- 20 T. C. Ho, *Catal. Rev.*, 1988, **30**, 117-160.
- 21 A. Hrabar, J. Hein, O. Y. Gutiérrez and J. A. Lercher, *J. Catal.*, 2011, **281**, 325-338.
- 22 O. Y. Gutiérrez, A. Hrabar, J. Hein, Y. Yu, J. Han and J. A. Lercher, *J. Catal.*, 2012, **295**, 155-168.
- 23 E. W. Stern, *J. Catal.*, 1979, **57**, 390-396.
- 24 R. M. Laine, *Catal. Rev.*, 1983, **25**, 459-474.
- 25 K. S. Liang, S. P. Cramer, D. C. Johnston, C. H. Chang, A. J. Jacobson, J. P. deNeufville and R. R. Chianelli, *J. Non-Cryst. Solids*, 1980, **42**, 345-356.
- 26 C. H. Chang and S. S. Chan, *J. Catal.*, 1981, **72**, 139-148.
- 27 S. J. Hibble, R. I. Walton, D. M. Pickup and A. C. Hannon, *J. Non-Cryst. Solids*, 1998, **232-234**, 434-439.
- 28 S. J. Hibble and G. B. Wood, *J. Am. Chem. Soc.*, 2004, **126**, 959-965.
- 29 H. G. S. Casalongue, J. D. Benck, C. Tsai, R. K. B. Karlsson, S. Kaya, M. L. Ng, L. G. M. Pettersson, F. Abild-Pedersen, J. K. Nørskov, H. Ogasawara, T. F. Jaramillo and A. Nilsson, *J. Phys. Chem. C*, 2014, **118**, 29252-29259.
- 30 M. L. Tang, D. C. Grauer, B. Lassalle-Kaiser, V. K. Yachandra, L. Amirav, J. R. Long, J. Yano and A. P. Alivisatos, *Angew. Chem.*, 2011, **123**, 10385-10389.
- 31 P. C. K. Vesborg, B. Seger and I. Chorkendorff, *J. Phys. Chem. Lett.*, 2015, **6**, 951-957.
- 32 W. Zhang, T. Zhou, J. Zheng, J. Hong, Y. Pan and R. Xu, *ChemSusChem*, 2015, **8**, 1464-1471.
- 33 G. Shi, W. Han, P. Yuan, Y. Fan and X. Bao, *Chin. J. Catal.*, 2013, **34**, 659-666.
- 34 K. Hu, X. Hu, Y. Xu and J. Sun, *J. Mater. Sci.*, 2010, **45**, 2640-2648.
- 35 K. H. Hu, Z. Liu, F. Huang, X. G. Hu and C. L. Han, *Chem. Eng. J.*, 2010, **162**, 836-843.
- 36 E. J. M. Hensen, V. H. J. de Beer, J. A. R. van Veen and R. A. van Santen, *Catal. Lett.*, 2002, **84**, 59-67.
- 37 E. J. M. Hensen, P. J. Kooyman, Y. van der Meer, A. M. van der Kraan, V. H. J. de Beer, J. A. R. van Veen and R. A. van Santen, *J. Catal.*, 2001, **199**, 224-235.
- 38 X. Ma, K. Sakanishi and I. Mochida, *Ind. Eng. Chem. Res.*, 1994, **33**, 218-222.
- 39 M. Jian and R. Prins, *J. Catal.*, 1998, **179**, 18-27.
- 40 J. Hein, A. Hrabar, A. Jentys, O. Y. Gutiérrez and J. A. Lercher, *ChemCatChem*, 2014, **6**, 485-499.
- 41 H. Vrubel, D. Merki and X. Hu, *Energy Environ. Sci.*, 2012, **5**, 6136-6144.
- 42 J. D. Benck, Z. Chen, L. Y. Kuritzky, A. J. Forman and T. F. Jaramillo, *ACS Catal.*, 2012, **2**, 1916-1923.
- 43 L. Qiu and G. Xu, *Appl. Surf. Sci.*, 2010, **256**, 3413-3417.
- 44 P. Afanasiev and I. Bezverkhyy, *Chem. Mater.*, 2002, **14**, 2826-2830.
- 45 Y. Fan, H. Xiao, G. Shi, H. Liu and X. Bao, *Energy Environ. Sci.*, 2011, **4**, 572-582.
- 46 Y. Fan, H. Xiao, G. Shi, H. Liu, Y. Qian, T. Wang, G. Gong and X. Bao, *J. Catal.*, 2011, **279**, 27-35.
- 47 I. Bezverkhyy, P. Afanasiev and M. Lacroix, *J. Catal.*, 2005, **230**, 133-139.
- 48 Q. Ji, Y. Zhang, Y. Zhang and Z. Liu, *Royal Soc. Chem.*, 2015, **44**, 2587-2602.
- 49 E. J. M. Hensen, Y. van der Meer, J. A. R. van Veen and J. W. Niemantsverdriet, *Appl. Catal. A*, 2007, **322**, 16-32.
- 50 S. Texier, G. Berhault, G. Pérot, V. Harlé and F. Diehl, *J. Catal.*, 2004, **223**, 404-418.
- 51 R. R. Chianelli, A. F. Ruppert, M. José Yácaman and A. Vázquez-Zavala, *Catal. Today*, 1995, **23**, 269-281.
- 52 Y. Okamoto, K. Ochiai, M. Kawano and T. Kubota, *J. Catal.*, 2004, **222**, 143-151.
- 53 L. Alvarez, J. Espino, C. Ornelas, J. L. Rico, M. T. Cortez, G. Berhault and G. Alonso, *J. Mol. Catal. A: Chem.*, 2004, **210**, 105-117.
- 54 F. Pedraza and S. Fuentes, *Catal. Lett.*, 2000, **65**, 107-113.
- 55 W. Trakarnpruk and B. Seentrakoon, *Ind. Eng. Chem. Res.*, 2007, **46**, 1874-1882.
- 56 Y. Okamoto, K. Hioka, K. Arakawa, T. Fujikawa, T. Ebihara and T. Kubota, *J. Catal.*, 2009, **268**, 49-59.
- 57 P. Afanasiev, *J. Catal.* 2010, **269**, 269-280.
- 58 M. Fang, W. Tang, C. Yu, L. Xia, Z. Xia, Q. Wang and Z. Luo, *Fuel Process. Technol.*, 2015, **129**, 236-244.
- 59 H. Topsøe, B. S. Clausen, N. Y. Topsøe and E. Pedersen, *Ind. Eng. Chem.*, 1986, **25**, 25-36.
- 60 P. Afanasiev, H. Jobic, C. Lorentz, P. Leverd, N. Mastubayashi, L. Piccolo and M. Vrinat, *J. Phys. Chem. C*, 2009, **113**, 4139-4146.

The origin of active sites of hydrodenitrogenation catalysts was comprehensively studied using alumina-supported MoS_3 nanoparticles (NPs) as a novel precursor.

